Revision 1

Authigenic anatase nanoparticles as a proxy for sedimentary environment and porewater pH

Hanlie Hong[1*], Kaipeng Ji[1], Chen Liu[1], Thomas J. Algeo[2,3,4], Ke Yin[1], Lulu Zhao[1], Michael F. Hochella Jr.[5], Qian Fang[1], Chaowen Wang[6]

[1] School of Earth Sciences, China University of Geosciences, Wuhan 430074, China
[2] State Key Laboratory of Biogeology and Environmental Geology, China University of Geosciences, Wuhan 430074, China
[3] State Key Laboratory of Geological Processes and Mineral Resources, China University of Geosciences, Wuhan 430074, China
[4] Department of Geology, University of Cincinnati, Cincinnati, OH 45221-0013, USA
[5] Department of Geosciences, Virginia Tech, Blacksburg, VA 24061, USA
[6] Gemological Institute, China University of Geosciences (Wuhan), Wuhan 430074, Hubei, China

*Corresponding author. Email: honghanlie@cug.edu.cn

ABSTRACT

Titanium (Ti) has long been considered to be immobile during weathering and diagenetic processes, and it is widely used for normalization of elemental concentrations in weathering profiles. However, our study demonstrates that authigenic titania is commonly formed in fine-grained siliciclastics of a wide variety of facies through weathering of Ti-bearing silicates, authigenic euhedral anatase is present ubiquitously as nanoparticles and its morphology varies in a predictable manner over a range of depositional environments. The crystal habit of authigenic anatase nanoparticles is controlled primarily by porewater pH during early diagenetic alteration of Ti-bearing silicates. Authigenic anatase nanoparticles exhibit a distinct tetragonal tabular morphology in deep-marine facies, a tetragonal bipyramidal shape in shallow-marine facies, an irregular morphology with sponge-like aggregates in terrestrial-marine transitional to paludal facies, and euhedral short tetragonal prisms in lacustrine facies. Also, authigenic anatase is observed to form in organic-free glacial deposits, attesting its formation as an inorganic precipitate and demonstrating diagenetic remobilization of titanium in the absence of organic matter. Our findings suggest that authigenic anatase could be a sensitive proxy for sedimentary environment and sedimentary porewater chemistry, and will likely prove useful in depositional facies analysis.

KEYWORDS: Anatase; nanoparticle; morphology; sedimentary facies; porewater chemistry

INTRODUCTION

Titania (TiO_2) occurs as three polymorphs, of which rutile is the thermodynamically most stable, and anatase and brookite are metastable at low temperatures and pressures and may transform to rutile, especially as demonstrated at the nanoscale (Zhang and Banfield, 2014). However, anatase is an exceedingly common authigenic form of titania in soils and detrital sediments generated during chemical weathering processes and diagenetic alteration, and occurring as nanosize titanium oxide particles ubiquitously in these geologic environments (Hochella et al., 2019). [Note: 'nanoparticles' in this context are small mineral particles in the size range of several tens of nanometers, or less, in at least one dimension (Hochella et al., 2008)]. Titanium (Ti) released from weathering/alterations of detrital sediments or rocks in colloidal form is usually associated with clay mineral aggregates (Banfield et al., 1991; Ece and Nakagawa, 2003), and hence, anatase nanoparticles in association with clay minerals generally originate from diagenetic alteration of volcanic glass and Ti-bearing minerals.

Authigenic minerals with significantly higher density than silicates and carbontes, such as TiO_2 polymorphes, persist in a wide variety of sedimentary facies through alteration and chemical weathering during early diagenesis. Their stability fields provide limits on the range of pH, Eh, and temperature conditions associated with their formation (Dill, 2010). Authigenic titania minerals, in particular, are chemically stable and form in various depositional environments, providing a useful proxy for assessment of diagenetic conditions (Weibel and Friis, 2004). Ti is relatively immobile in supergene environments and is often employed as a reference element to evaluate the mass flux of other mobile elements owing to the resistance to weathering of Ti-oxide minerals and the exceptionally low solubility of Ti in aqueous solution (Young and Nesbitt, 1998). However, there is evidence showing that Ti is mobile during hydrothermal alteration and can precipitate as low-temperature titania phases, with dissolution of Ti often associated with the presence of strong complexing ligands, especially those of organic acids (Schulz et al., 2016). Overall, the formation of authigenic anatase nanoparticles in sediments challenges long-standing assumptions regarding the crystallographical habits and geochemical behavior of Ti, yet this process remains poorly understood.

To better delineate the crystallographical habits and geochemical behavior of authigenic anatase

and to assess its suitability as a proxy for diagenetic conditions and sedimentary facies, this study investigates anatase nanoparticles formed in fine-grained siliciclastic sediments (ash beds and detrital mudstones) of Permian-Triassic boundary (PTB) successions in South China representing various depositional environments. This region provides ideal conditions to study variation in authigenic anatase across multiple sedimentary facies because of the presence of fine-grained detrital sediments with interbedded volcanic ash beds in a range of settings, including deep marine, shallow marine, nearshore littoral, terrestrial-marine transitional, paludal, and lacustrine (Fig. 1; Hong et al., 2019). Ash beds with uniform initial compositions deposited across a range of depositional environments can facilitate study of the effects of facies-specific porewater conditions on authigenic anatase formation. To broaden the range of environments studied and enhance the potential global significance of our findings, we also investigated authigenic anatase in Cryogenian (~720–635 Ma) glacial deposits lacking organic matter.

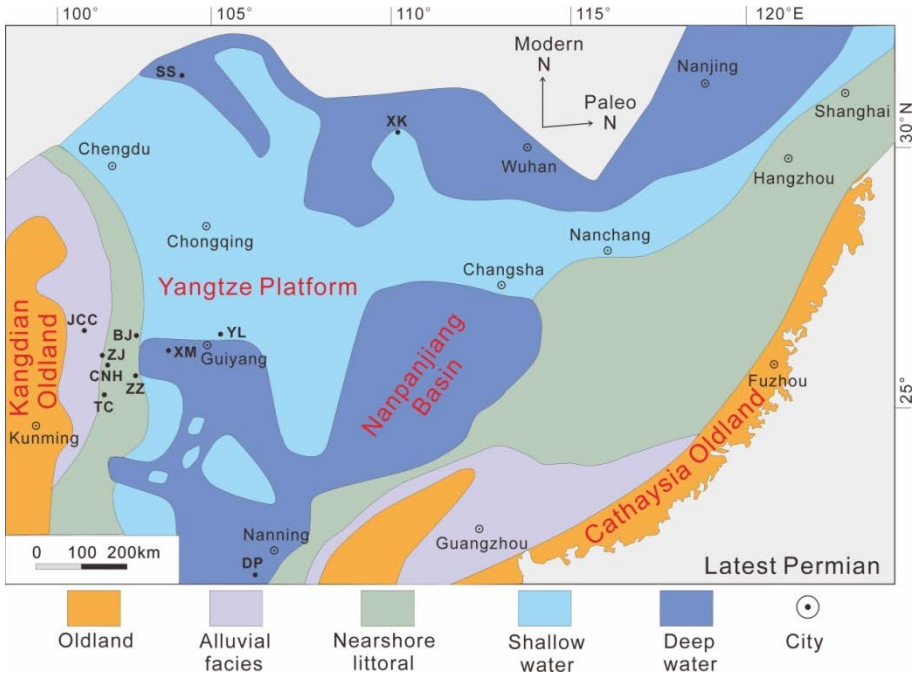

Fig. 1. Paleogeographic map of South China in the latest Permian showing sedimentary facies. Deep-marine sections: Xinmin (XM), Dongpan (DP), Shangsi (SS); Shallow-marine to nearshore littoral sections: Yanlou (YL), Xiakou (XK), Zhongzhai (ZZ), Zhejue (ZJ), Chinahe (CNH); Lacustrine sections: Jiucaichong (JCC); Paludal to terrestrial-marine transitional sections: Bijie (BJ) and Tucheng (TC). Modified from Hong et al. (2019).

SAMPLING

87 *Sampling*

88 Samples, each weighing ~500 g, were collected from well-studied Permian-Triassic boundary
89 (PTB) sections of known sedimentary facies for our investigation, in order to avoid uncertainty in
90 environmental assignments (Fig. 1). Volcanic ash samples were collected from all study sections,

91 Table 1 Depositional facies and location of the study samples

Depositional facies	Section	Location	Sampling
Deep water	Xinmin (XM)	Xinmin village, Puding county, Anshun city, Guizhou Province (26°23'55"N, 105°57'16"E)	Ash
	Shangsi (SS)	Shangsi village, Jiange county, Guangyuan city, Sichuan Province (32°10'05"N,105°18'02"E)	Ash
	Dongpan (DP)	Dongpan village, Liuqiao town, Liuqiao county, Chongzuo city, Guangxi Province (22°16.20"N,107°41.50"E)	Ash, detrital mudstone
Shallow water to nearshore littoral	Zhongzhai (ZZ)	Zhongzhai town, Liuzhi district, Liupanshui city, Guizhou Province (26°9'10″N, 105°17'11″E)	Ash
	Xiakou (XK)	Xikou town, Xingshan county, Hubei Province (31°6′51″N, 110°48′13″E)	Ash, detrital mudstone
	Yanlou (YL)	Yanlou district, Guiyang city, Guizhou Province (26°20'14"N,106°38'30"E)	Ash
	Zhejue (ZJ)	Zhejue village, Weining county, Guizhou Province (26°35'25"N, 103°55'56"E)	Ash
	Chinahe (CNH)	Baiyi village, Tianba Town, Xuanwei City, Guizhou Province (26°7′35″N, 104°21′6″E)	Ash
Lacustrine	Jiucaichong (JCC)	Jiucaichong village, Heishitou town, Weining county, Guizhou Province (26°43'9"N, 104°0'1"E)	Ash
Terrestrial-marine transitional to paludal	Tucheng (TC)	Tucheng town, Panxian county, Guizhou Province (25°51'58"N, 104°27'32"E)	Ash
	Bijie (BJ)	Changzheng village, Bijie City, Guizhou Province (27°21′49″N, 105°21′3″)	Ash
Nantuo glacial deposits	Jiulongwan (JLW)	Jiulongwan village, Sandouping Town, Zigui County, Yichang City, Hubei Province (30°48′145″N, 111°3′19″E)	Detrital mudstone
	Gucheng (GC)	Gucheng village, Gaojiayan Town, Changyang County, Yichang City, Hubei Province (30°33′21″N, 111°3′16″E)	Detrital mudstone

whereas the associated background detrital mudstones were collected only from the deep-marine Dongpan (DP) section and the shallow-marine Xiakou (XK) section, taking into account the generally rapid changes in sedimentary facies of lacustrine and paludal sections. The depositional facies and sampling locations of the samples studied are listed in Table 1.

Ash samples with the numbers of 11, 12, and 2 were collected from the XM, DP, and SS sections respectively, and 17 associated background detrital mudstones were collected from the SS section for the deep-marine study unit. For the shallow-marine to nearshore littoral study units, ash samples with the numbers of 2, 7, 6, 2, and 2 were collected from the ZZ, XK, YL, ZJ, and CNH sections, respectively. Fourteen associated background detrital mudstones were collected from the XK section. Only one ash bed was identified and collected in the JCC and BJ sections, and 3 ash samples were collected from the TC sections, respectively.

For a case study of the use of anatase as a proxy for sedimentary facies, samples were also collected from mudstones of the Nantuo Formation glacial deposits in the Jiulongwan and Gucheng sections. In the Jiulongwan (JLW) section the Nantuo glacial deposits have a thickness of about 200 meters, while in the Gucheng (GC) section they have a thickness of only a few tens of meters (Hu et al., 2020). Six mudstone samples from JLW and two from GC were collected for this study.

METHODS

X-ray diffraction

The whole-rock samples were dried in an electric oven at 60 °C overnight and then ground with a mortar and pestle to powder finer than 200 mesh. The whole-rock samples were prepared by mounting the powder into a sample holder using a back-press technique. The < 2 μm clay fraction was extracted by sedimentation and centrifugation methods, and the oriented clay sample was prepared by pipetting the extracted clay suspension onto a glass slide and allowing it to air-dry at room temperature. The X-ray diffraction (XRD) analysis was performed on a Panalytical X'Pert PRO DY2198 diffractometer at the State Key Laboratory of Geological Processes and Mineral Resources, China University of Geosciences (Wuhan). The instrument was operated at 35 kV voltage and 30 mA current with Ni-filtered Cu (Kα = 1.541874 Å) radiation, and a slit system with 1° divergence slit, 1° anti-scatter slit, and 0.3 mm receiving slit. The XRD patterns were collected

from 3 to 65° 2θ at a scan rate of 4° 2θ/min.

HRTEM analysis

High-resolution transmission electron microscopy (HRTEM) was undertaken in order to characterize the morphology and lattice fringe spacings of individual anatase nanoparticles. The extracted clay fraction of the sample was immersed in methanol and dispersed with ultrasonic waves for a period of 10 min, and subsequently collected with a copper net and then dried under infrared light. Observations were performed on a FEI TECNAI G2 S-TWIN field-emission HRTEM equipped with an EDAX solid-state EDX detector and a Gatan 830 charge-coupled device (CCD) camera system at the Shanghai Institute of Measurement and Testing Technology. The instrument was operated at an accelerating voltage of 200 kV, with a point-to-point resolution of 0.24 nm and a line resolution of 0.14 nm. Under the HRTEM, the electron density contrast of the mineral particles is dominantly dependent on its atomic mass/chemical composition and grain thickness. Images of anatase particles with relatively darker color are indicative of greater grain thickness. During observation, anatase particles were first identified using EDS at lower magnification and then imaged at higher magnification. The area selected for electron diffraction was usually at the thin edge of each anatase grain. The diffraction patterns were analyzed using the Digital Micrograph software version 3.9 (Gatan Ltd.) and compared to standard diffraction patterns of anatase (PDF#21-1272; space group: $I4_1/amd$; cell parameters: $a_0=b_0=3.7852$ Å, $c_0=9.5139$ Å).

SEM observation

Occurrence of anatase nanoparticles in ash samples were observaed by scanning electron microscope (SEM). Small chips of selected bulk samples with ~0.5 cm in size were fixed on a sample holder and coated then with carbon. SEM observation was undertaken on a SU8010 field emission scanning electron microscope, equipped with an energy dispersive spectrometer (EDS) in order to provide the assistance of chemical composition for identification of small mineral particles during microscopic observation. The instrument was operated at an accelerating voltage of 20 kV and a beam current of 80 to 100 nA at the Faculty of Materials Science and Chemistry of China University of Geosciences (Wuhan), with a resolution of secondary electron image of 1.0

nm.

RESULTS

Due to the relatively low abundance of anatase in the clay fractions of the study samples, its presence can be detected by X-ray diffraction (XRD) analysis only occasionally (Fig. 2). However, high-resolution transmission electron microscopy (HRTEM) showed that anatase was commonly present as single crystals with a size of tens to hundreds of nanometers. The morphology of the anatase particles exhibits only limited variation within a single section or between different sections of the same sedimentary facies, but it varies considerably across facies.

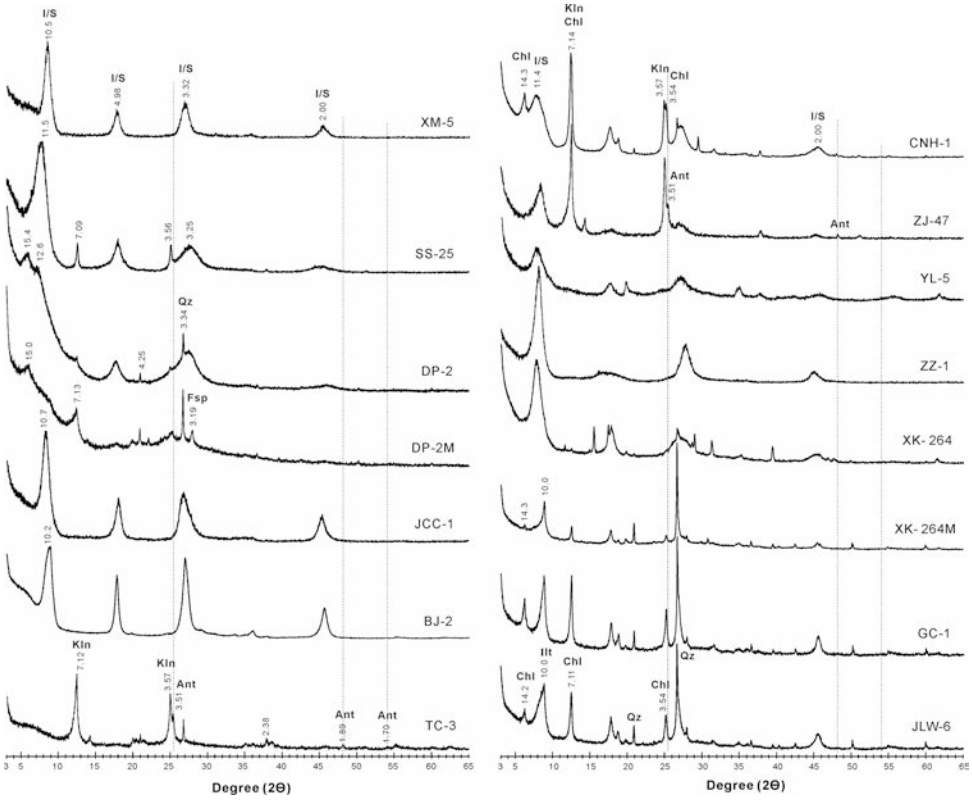

Fig. 2. XRD patterns showing the clay phases of sediments and associated anatase. I/S: mixed-layer illite/smectite; Kln: kaolinite; Ilt: illite; Chl: chlorite; Qz: quartz; Fsp: feldspar; Ant: anatase. DP-2M: background mudstone from the DP section; XK-264M: background mudstone from the XK section.

In deep-marine facies, most anatase nanoparticles have an euhedral tetragonal and short prism morphology which provides a square or rectangular cross-section depending on the exact orientation to the electron beam, with particle sizes mostly ranging from 30 to 200 nm in their largest dimension (mean ~100 nm) (Fig. 3). Only relatively rare particles were observed in shapes

other than this, often with rounded edges (Fig. 1D), or, in aggregates. Anatase crystals at XM exhibit relatively larger sizes as reflected by their darker contrast and often straighter edges, compared to those in the SS and DP sections. Anatase nanoparticles from the mudstone samples show similar characterictics to those in the adjacent ash deposits, indicating that their morphology was dependent on depositional facies but not on lithology. For example, mudstones of the deep-water DP section yield anatase crystals 30 to 120 nm in diameter, having a tetragonal tabular shape, and occasionally rounded margins due to lower Ti concentrations (Hong et al., 2019).

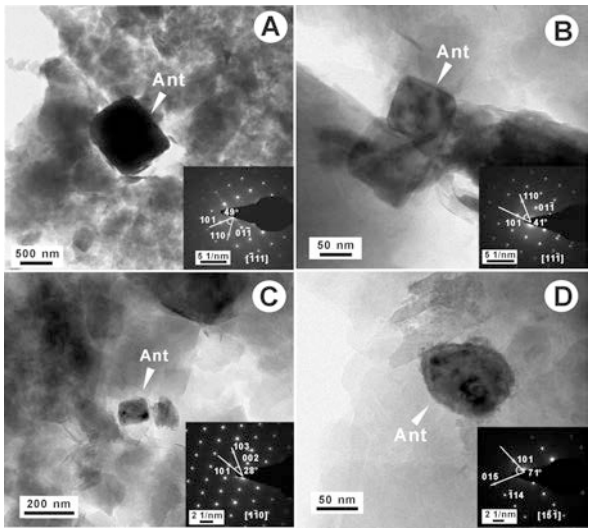

Fig. 3. Authigenic anatase (Ant) in samples of deep-water sections showing nanoparticles of typically tetragonal tabular shape. (A) Xinmin ash, XM-5; (B) Shangshi ash, SS-25; (C) Dongpan ash, DP-2; (D) Dongpan mudstone, DP-RM.

In shallow-marine to nearshore littoral facies, anatase exhibits a morphology unlike that observed in the deep-marine deposits. Crystals formed in shallow waters are dominantly tetragonal bipyramidal in shape with generally straight margins, with only minor differences between sections (Fig. 4). Occassionally, anatase crystal with 1-2 irregular edges could also be observed in the shallow-marine samples. Particle size usually ranges from 80 to 300 nm (mean ~150 nm), being larger than crystals from deep-marine deposits. Due to the relatively better development of {001} and {101} compared to {100} faces, anatase sometimes forms truncated tetragonal bipyramidal crystals, some having a pseudo-hexagonal shape elongated in the [101] direction. Anatase in the lagoonal CNH section displays well-developed truncated tetragonal bipyramids, analogous to crystals of the nearshore littoral ZZ section. Shallow-marine mudstones of the XK section yield anatase having short, truncated tetragonal bipyramidal to

pseudo-hexagonal shapes with straight margins, similar to those in the adjacent ash beds.

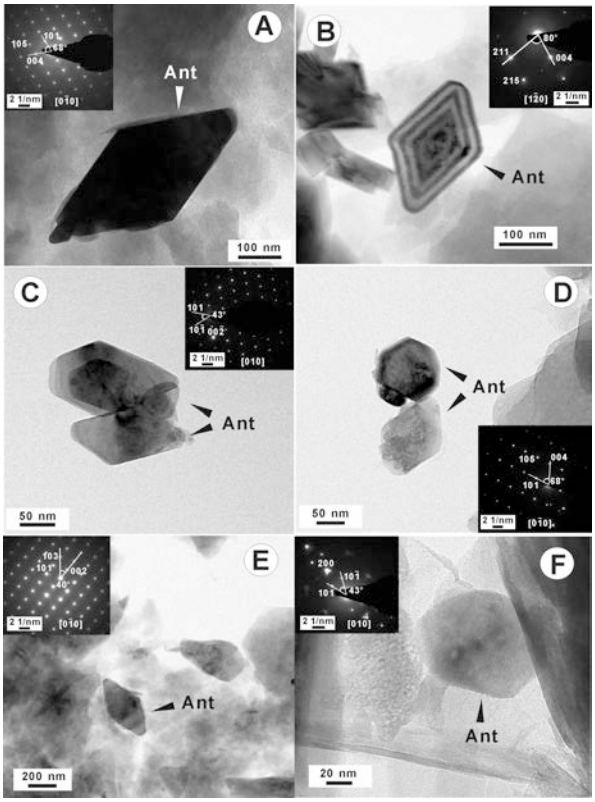

Fig. 4. Authigenic anatase in shallow-marine to nearshore littoral sediments showing nanoparticles of typically tetragonal bipyramidal and truncated tetragonal bipyramidal shapes. (A) Zhongzhai ash, ZZ-1; (B) Xiakou ash (the pseudogirdle structure derived from equal thickness interference), XK-264; (C) Yanlou ash, YL-5; (D) Zhejue ash, ZJ-47; and (E) Chinahe ash, CNH-1; (F) Xiakou mudstone, XK-264M.

In terrestrial-marine transitional to paludal facies, anatase shows a distinctively irregular morphology (Fig. 5A,B). The crystals formed in this environment are mainly 70 to 150 nm in diameter and have dominantly irregular shapes with extremely rare straight edges and, more rarely, elongated ellipsoidal shapes or aggregates of sponge-like shapes, which have been interpreted to form due to oriented attachment during phase transformation of $Ti(OH)_4$ colloids in the presence of organic ions (Sugimoto et al., 2003; Gallego-Urrea et al., 2014). The morphology of anatase aggregates shows minor variation between different sections, e.g., anatase in the paludal BJ section displays anhedral sponge-like aggregates, and single crystals with well-defined edges are absent, whereas in the terrestrial-marine transitional TC section it occurs dominantly in aggregates of smaller ellipsoidal and anhedral grains, and even occasionally as tetragonal bipyramidal crystals.

In lacustrine facies, anatase occurs typically as euhedral short tetragonal prisms with straight edges and occasionally with slightly round edges (Fig. 5C,D). Crystal size ranges mostly from 80 to 400 nm. Nearshore lacustrine environments are open and exoreic (Inglès and Ramos-Guerrero, 1995), with a watermass that is either exchanged with seawater (i.e., lagoonal) or isolated from the ocean (i.e., closed lacustrine). Anatase in the JCC section of closed lacustrine environment is present usually in cuboid shape with slightly round edges, different from that of the lagoonal CNH environment.

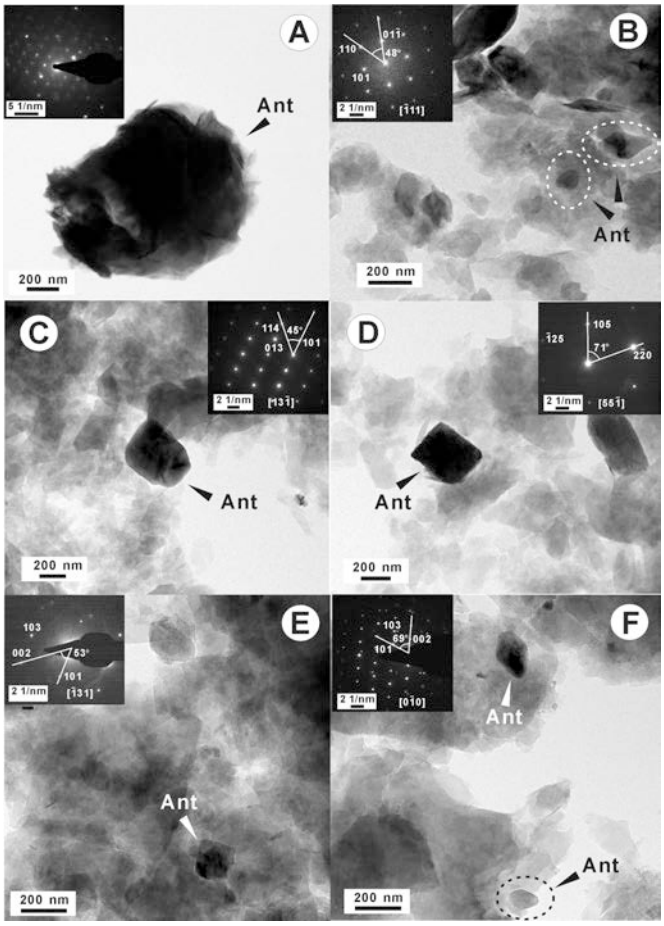

Fig. 5. Authigenic anatase in representative samples of lacustrine and terrestrial-marine transitional to paludal facies and in glacial mudstones. (A) Sponge-like aggregates in paludal Bijie ash (anatase multi-crystal diffraction ring of), BJ-1; (B) Anhedral and occasionally tetragonal bipyramidal shapes in terrestrial-marine transitional Tucheng ash, TC-3; (C), (D) Cuboid shapes in lacustrine Jiucaichong ash, JCC-1; (E), (F) Authigenic anatase in Jiulongwan (JLW-6) and (F) Gucheng (GC-1) glacial mudstones showing distinctive morphologies consistent with lacustrine and shallow-water environments, respectively.

In the JLW glacial deposits, authigenic anatase nanoparticles are generally euhedral short

tetragonal prisms with relatively straight edges and, in some cases are rounded and irregular shapes, with a grain size of 40-150 nm, similar to the morphology of anatase in lacustrine facies (Fig. 5E,F). However, anatase in the GC glacial deposits has a diameter of 80-200 nm and exhibits a uniquely truncated tetragonal bipyramidal morphology with only occasional presence of rounded and irregular outlines, similar to those of shallow-marine facies and different from those in the JLW glacial deposits.

Backscattered electron microscopic analysis of the Xiakou ashes suggest that Ti-bearing materials (probably anatase) with tens of micrometers in size occur occasionally in the samples (Fig. 6). The Ti-bearing materials are usually confined within the detrital particles. Although lack of direct evidence for potential precursor of the Ti-bearing materials, the overlapped Ti-, Zr-mapping in association with the presence of trace Ca in the particles suggest a likely precursor of uhligite. The chemical composition of dominantly Ti and Zr with trace Ca for the detrital particles is indicative of weak alteration and thus incomplete leaching of Ca from the particles. However, at a distance of usually <10 μm surrounding the detrital particles there are aggregates of tiny spheroidal Ti grains in the microfissures, suggesting a colloidal precipitation of TiO_2 phases due to weathering of the detrital Ti-bearing particles.

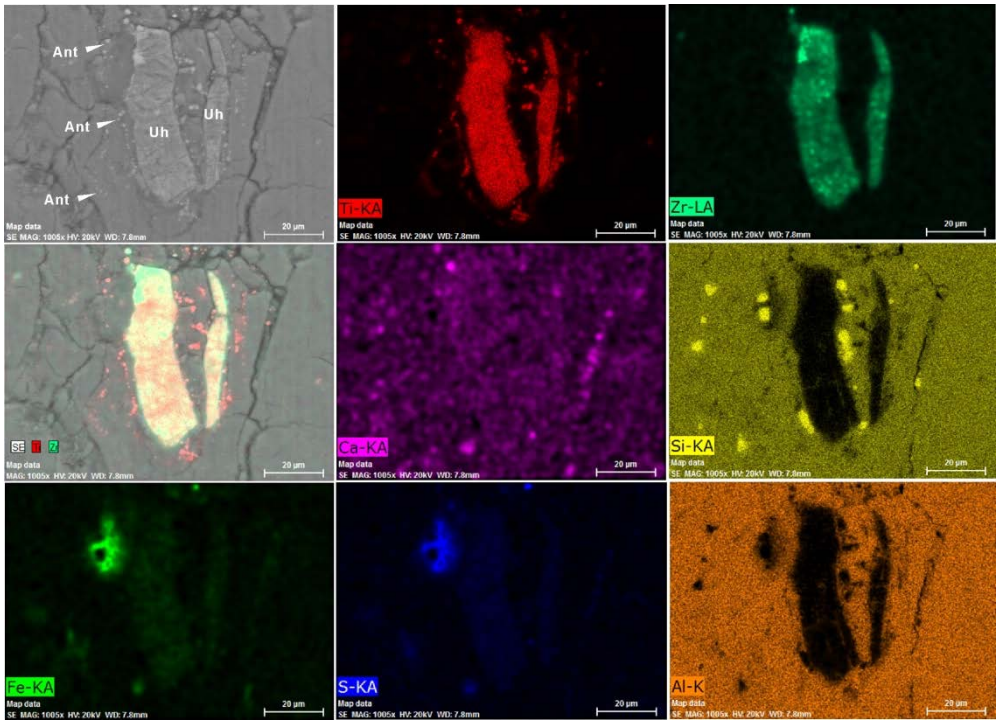

Fig. 6. Element mapping of the XK-264 ash sample showing detrital Ti-bearing mineral uhligite (Uh) and the neoformed TiO_2 (anatase) aggregates.

DISCUSSION

Facies dependence of authigenic anatase

Titanium is generally incorporated in early-precipitated magmatic minerals such as biotite, amphibole, and pyroxene. However, Ti-bearing accessory minerals are rare in marine sediments owing to their high density (3.8–4.3 g/cm^3), which leads to mechanical sorting and impedes their transport to distal marine basins (Abdel-Rahman, 1994; Schulz et al., 2016). Although Ti is considered to be relatively immobile, research has shown that Ti can be released from Ti-bearing detrital phases, migrate, and reprecipitate in authigenic phases during early diagenesis (Banfield et al., 1991; Tilley and Eggleton, 2005; Baioumy, 2014). Authigenic anatase often takes the form of euhedral nanoparticles. Rounding of the margins of anatase nanocrystals may suggest conditions reflecting undersaturation of porewaters with respect to titania during crystal growth and, thus, resulting in rounded crystal edges and corner, and at higher even dilution, spherical nanocrystals (Gao and Elder, 2000). The average TiO_2 content of ash beds in PTB sequences of South China decreases from paludal (5.24%) to lacustrine (1.31%), and then to shallow- (0.44%) and deep-marine facies (0.54%) (Hong et al., 2019). The ash beds of marine facies contain significantly less Ti, especially in sections such as DP and SS (Hong et al., 2019).

Anatase nanoparticles exhibit distinctive euhedral morphologies in both ash and regular sedimentary host rocks except for samples of the paludal facies, suggesting that anatase is an authigenic mineral formed from solution during alteration of precursor materials (Zhang and Banfield, 1998). The uniform character of nanoparticles in the same sedimentary environment indicates an *in situ* authigenic origin, and the similar morphologies of anatase crystals in a given sedimentary facies, regardless of source material, age, and locality, suggest crystallization controlled by pore-water conditions, which were closely linked to specific sedimentary facies (Baioumy, 2014). Ti can be released from the weathering of glassy material and Ti-bearing silicate minerals (e.g., biotite, clinopyroxene, and amphibole) through alteration, and released Ti can subsequently recrystallize as anatase (Fontaine et al., 2020). Except for glassy material, detrital Ti-bearing silicate minerals may be the main source of Ti for post-depositional alteration reactions (Liu et al., 2019). Therefore, the morphology of anatase nanoparticles is sensitively dependent on the physical and chemical conditions of sediment pore waters in various depositional

environments during early diagenesis.

Lack of characteristic biofacies in these units makes it difficult to identify specific sedimentary environments. Based on investigation of variations in thickness and lithology of the glacial deposits at different sites, it has been inferred that the sediments formed as subglacial deposits in the northeast and transitioned into glaciomarine deposits in the southwest, with deposition of the JLW section in an inner shelf environment (glacial marginal lake) and the GC section in a shallow-marine environment (Hu et al., 2020). Our authigenic anatase data provide another line of evidence of sedimentary conditions and validates differences in sedimentary environments between the two sections (Fig. 5E,F). Similar observations reported elsewhere also suggested that the morphology of authigenic anatase is facies-dependent. In lacustrine and shallow-marine sequences of sedimentary rocks in southern and central Sweden, authigenic anatase exhibits an acute bipyramidal habit in the pore spaces of shallow-marine sediments, but it displays a distinct small cuboid-like morphology in lacustrine deposits (Morad and Aldahan, 1982). In the kaolinite-bearing Huber Formation of eastern Georgia, which was deposited in freshwaters (pH 7-8) of inter-deltaic and estuarine settings, anatase was observed to form cubic-like nanocrystals in close association with kaolinite particles (Schroeder and Shiflet, 2000).

Porewater chemistry controlling crystal morphology of authigenic anatase

Ti has a low solubility under both oxic and anoxic conditions and is usually present in a single valence state (4+). It is believed to be inert to redox changes in seawater, and the formation and stability of anatase are not sensitive to temperature and pressure (Skrabal, 2006; Barnard and Xu, 2008). The morphology of anatase is largely controlled by the solution pH, which influences the adsorption of Ti aqueous ions on different crystallographic faces of the TiO_2 nucleus and, thus, controlling the shape of the final authigenic crystals (Sugimoto et al., 2003; Símonarson et al., 2019). Solution pH exerts a strong influence on surface free energies (γ), whose values for the {001}, {100}, and {101} sets of crystal faces for anatase change significantly and differently among the different faces as pH varies from highly acidic to highly basic. The ratios of γ for different pairs of faces for highly acidic, moderately acidic, neutral, moderately basic, and highly basic solutions are as follows: those of $\gamma_{101/001}$ are 0.61, 0.62, 0.66, 0.79, 0.81, those of $\gamma_{101/100}$ are 0.81, 0.84, 0.91, 0.95, and 1.35, and those of $\gamma_{100/101}$ are 1.24, 1.18, 1.10, 1.05, and 0.74, all from

low the high pH (Barnard et al., 2005). Because a smaller surface free energy represents relatively greater stability of a crystal surface, the ratios of the free energies of crystal surfaces are likely to reflect their relative degree of development. Therefore, acidic solutions favor formation of {101} facets due to its relatively smaller surface free energy compared to those of the {001} and {100} facets, whereas basic conditions favor {001} facets relative to the {101} and {100} facets. As a result, anatase is generally present with a square-like tretagonal morphology under basic conditions and with a tetragonal bipyramidal morphology under acidic solutions. Previous experiments showed that anatase can crystallize from titanium colloids in a wide range of environments from mildly acid to neutral and alkaline hydrothermal solutions (Matthews, 1976; Tilley and Eggleton, 2005). Thus, in natural geological environments, the stability and growth shape of titania are mainly controlled by pore-water pH (Zhang and Banfield, 2014).

Depositional environment strongly influences porewater chemistry and, thus, the post-depositional weathering of sediments (Khalifa and Morad, 2015). Organic-rich soil waters are generally acidic and have pH values of 4-7, whereas riverwater is moderately basic and has a pH value of 7-8 (Witham et al., 2005). In a closed lacustrine environment, porewater cation concentrations are often elevated, in part due to evaporation during dry periods and in part due to dissolution of sediments, raising porewater pH (Ddani et al., 2005). Seawater pH varies with water depth, decreasing from ~8.4 in the surface layer to ~7.4 below the thermocline (>200 m), and then increasing again to ~8.0 in the deep watermass. The surface layer is relatively basic due to the uptake of CO_2 by biological productivity, whereas in shallow-marine sediments, oxidation of sedimentary sulfide minerals in interstitial waters can strongly enhance the production of H^+ and acidify porewaters during early diagenesis (Pirlet et al., 2012). In the deep watermass, oxygen levels are commonly low, and anaerobic oxidation of organic matter causes a shift to more basic porewater conditions. Higher porewater pH is also promoted by increases in alkalinity within the zone of sulfate reduction, where H^+ is removed as H_2S gas, and through dissolution of fresh unstable carbonates, which consumes H^+ (Coleman, 1985).

As described above, euhedral anatase in sediment pores is generally authigenic in origin, formed via alteration of Ti-bearing precursors. For volcanic ash materials, which are relatively soluble upon deposition, Ti-bearing detrital silicates also decompose during early diagenesis (Hong et al., 2019; 2020). However, the degree of supersaturation of Ti exerts largely on

precipitation of TiO_2 minerals, as the concentration decreases the formation of TiO_2 minerals will be rutile, brookite, and then anatase (Símonarson, et al., 2019). Our HRTEM evidence show that TiO_2 grains associated with clay minerals are anatase phase, reflecting that precipitation of TiO_2 minerals took place at a low degree of Ti-supersaturation, also this circumstance would allow the formation of euhedral anatase crystals. On the contrary, as shown in our SEM observations (Fig. 6), dissolution of Ti-bearing precursors during diagenetic alteration would be expected to produce a locally higher degree of Ti-supersaturation, facilitating the formation of spheroidal grains of TiO_2 minerals. Mineral dissolution and the subsequent crystallization of anatase occur under nearly closed conditions, controlled dominantly by sediment porewater chemistry (Ddani et al., 2005; Baioumy, 2014). Since the porewaters of shallow-marine, lacustrine, and deep-marine sediments are usually acidic, moderately basic, and highly basic, respectively, a precise distinction between these early diagenetic facies can be made according to the morphology of authigenic anatase nanoparticles (Fig. 7). Slight differences in anatase crystal shape between localities representing the same depositional facies are related to small variations of porewater pH. For example, the thicker tetragonal tabular shapes at XM formed under more weakly basic conditions than those of the thinner shapes at SS and DP, and the acute bipyramidal shapes at XK, ZZ, and CNH formed under relatively more acidic conditions compared to the truncated tetragonal bipyramid shapes at YL and ZJ.

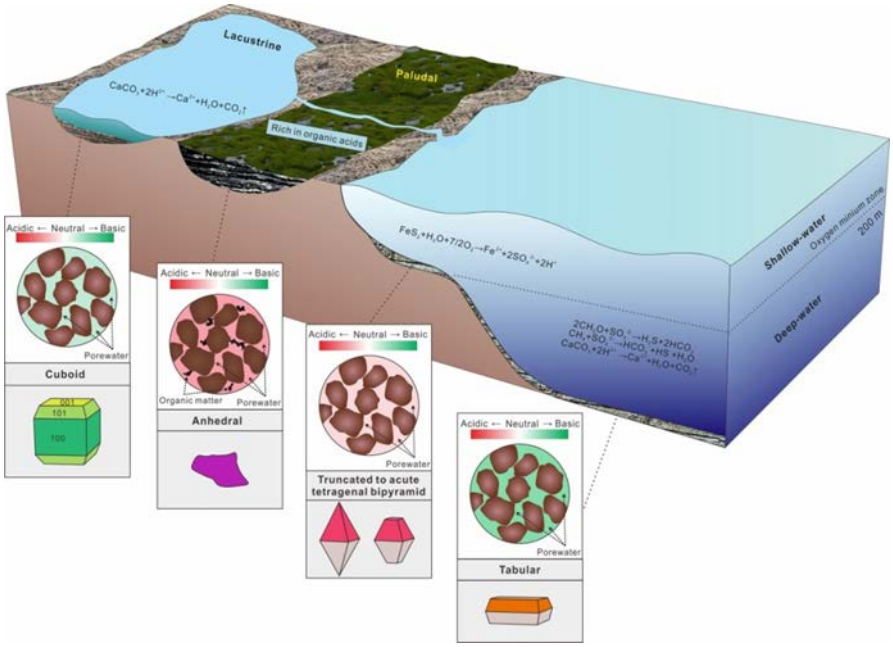

Fig. 7. The facies-dependent morphology of authigenic anatase nanoparticles, as controlled by sedimentary

353 porewater pH.

354 In sedimentary porewaters, the solubility and migration of Ti is often controlled by organic
355 acids (Strietzel et al., 1998; Cabral et al., 2012). TiO_2 is insoluble at pH > 2.5 and needs strongly
356 acidic conditions to mobilise Ti from primary titania minerals, and decay of organic matter in
357 sediments is the widely invoked mechanism for producing conditions favorable to authigenic
358 titania (Brookins, 1988; Liu et al., 2019). Formation of authigenic anatase is generally associated
359 with organic acids linked due to hydrocarbon generation during diagenesis, decreasing porewater
360 pH and generating a micro-environment facilitating the dissolution of detrital Ti-bearing minerals
361 (Pe-Piper et al., 2011; Schulz et al., 2016). In soils and sediments, especially in mudstones,
362 organic acids also commonly serve as a chelator in mobilizing Ti^{4+} because of their relatively high
363 abundance (Lovley et al., 1996; Pe-Piper et al., 2011). However, deposition of Ti under
364 organic-rich conditions usually produces aggregates of anhedral anatase grains (Liu et al., 2019),
365 since TiO_2 colloidal nanometer-sized grains tend to aggregate more intensely in the presence of
366 organic (e.g., humic and fulvic) acids. In the paludal BJ and TC sections in which organic matter
367 is notably abundant, anatase was present dominantly as aggregates of distinctively anhedral
368 particles, consistent with observations for similar facies elsewhere (Liu et al., 2019).

369

370 *Use of authigenic anatase as a pore-water pH and depositional facies proxy*

371 In organic-poor mudstones deposited in lacustrine and basin environments in which detrital
372 titania minerals are rare due to density-driven sorting, Ti is mainly present in detrital silicates.
373 Diagenesis in such sediments occurs dominantly in association with solutions from meteoric water
374 and the authigenic euhedral anatase would be expected to result from inorganic precipitation
375 processes during post-deposition to early diagenesis stages (Tilley and Eggleton, 2005). Anatase
376 can also be the product of supergene weathering of silicates under neutral pH conditions (Tilley
377 and Eggleton, 2005; Baioumy, 2014). Ti is released from silicates during early diagenesis, and
378 anatase is precipitated through leaching of alkali phases during silicate alteration (Schroeder and
379 Shiflet, 2000; Dill, 2010; Chaikovskiy et al., 2019). In a recent study of ash deposits in the TC
380 section, detrital titania grains with a size of >100 μm were observed in association with authigenic
381 euhedral anatase nanoparticles, suggesting that the authigenic euhedral anatase probably derived
382 from alteration of Ti-bearing silicates instead of titanium oxide minerals (Hong et al., 2020), since

383 the titania phases were usually insoluble and alteration of these minerals might occur dominantly
384 in late diagenesis (Strietzel et al., 1998; Cabral et al., 2012). Under these circumstances, anatase
385 usually formed euhedral nanoparticles in the pore space of the host sedimentary rocks. In
386 particular, authigenic anatase in the organic-matter free glacial deposits indicate the
387 overestimation of titanium mobility by organic matter.

388 In general, recognition of the distributional pattern of the sedimentary deposits in a region
389 requires essentially fundamental geological work such as sedimentary facies and paleogeography,
390 fossiliferous strata, and tectostratigraphy to establish correctly the stratigraphical frame and the
391 inherent stratigraphical sequences. The facies-specific morphology of authigenic anatase can
392 provide important insights into the porewater chemistry of sediments during early diagenesis and
393 has the potential to provide a reliable facies marker, particularly when lithologic and sedimentary
394 structural information are insufficient for this purpose, as is the case in some Precambrian
395 sedimentary environments. In addition, the unique behaviors of authigenic anatase may also be
396 useful as a tool for other purposes, such as estimating the time of gas and oil migration and
397 accumulation and interpreting the diagenetic history of siliciclastic rocks (Morad and Aldahan,
398 1982). Even though authigenic anatase is volumetrically insignificant in many sediments, its
399 presence can be readily determined via HRTEM analysis of the clay fraction.

400 The ubiquitous occurrence of authigenic anatase nanoparticles in sediments is evidence of the
401 widespread mobility of Ti under low-temperature conditions. Although it is generally believed that
402 anatase is the first TiO_2 phase to crystallize due to its relatively low surface energy, and that it
403 transforms into the more stable phase brookite when its size exceeds ~11 nm (Zhang and Banfield,
404 2014), anatase is the stable phase of nanoparticles formed in a wide range of varying pH at
405 low-temperature (from highly acidic to highly basic), and it can persist stably in many geologic
406 environments (soils and sediments) over geologic time (Barnard and Xu, 2008; Hochella et al.,
407 2019). The formation and stability of metastable titania phases is probably attributable to the
408 low-Ti precursor concentration in the sediments, the effect of the chemical environment on the
409 nanoparticles, and the physical association with clay surfaces, which may contribute significantly
410 to the relative thermodynamic stability of these phases (Szczepanik, 2017; Símonarson et al.,
411 2019).
412

IMPLICATIONS

Anatase characteristically has a tetragonal tabular morphology and a cubic- or rectangular-like shape in deep-marine facies, a tetragonal bipyramidal shape with generally straight margins in shallow-marine facies, an irregular morphology with sponge-like aggregates in terrestrial-marine transitional to paludal facies, and euhedral short tetragonal prisms with straight edges in lacustrine facies. Crystal habit is controlled mainly by the environment-dependent porewater pH during early diagenetic alteration of Ti-bearing silicates. In case of organic-free glacial deposits, authigenic anatase is also observed to form as euhedral nanoparticles with clear facies-dependent morphology, indicating that diagenetic remobilization of titanium and precipitation of authigenic anatase could occur as an inorganic process. These findings open up a new avenue of analysis of sedimentary porewater chemistry, and may even prove useful in depositional facies analysis where lithologic and sedimentary structural data are insufficient.

REFERENCES

Abdel-Rahman, A.M. (1994) Nature of biotites from alkaline, calc-alkaline, and peraluminous magmas. Journal of Petrology, 35, 525–541.

Baioumy, H.M. (2014) Ti-bearing minerals in sedimentary kaolin deposits of Egypt. Applied Clay Science, 101, 345–353.

Banfield, J.F., Jones, B.F., Veblen, D.R. (1991) An AEM-TEM study of weathering and diagenesis, Abert Lake, Oregon: I. Weathering reactions in the volcanics. Geochrmica et Cosmochimica Acta, 55, 2781–2793.

Barnard, A.S., and Xu, H.F. (2008) An environmentally sensitive phase map of titania nanocrystals. ACS Nano, 2, 2237–2242.

Barnard, A.S., Zapol, P., Curtiss, L.A. (2005) Anatase and rutile surfaces with adsorbates representative of acidic and basic conditions. Surface Science, 582, 173–188.

Brookins, D.G. (1988) Eh–pH Diagrams for Geochemistry. Springer-Verlag, Berlin, 176 p.

Cabral, A.R., Reith, F., Lehmann, B., Brugger, J., Meinhold, G., Tupinambá, M., Kwitko-Ribeiro, R. (2012) Anatase nanoparticles on supergene platinum–palladium aggregates from Brazil: Titanium mobility in natural waters. Chemical Geology, 334, 182–188.

Chaikovskiy, I.I., Chaikovskaya, E.V., Korotchenkova, O.V., Chirkova, E.P., Utkina, T.A. (2019)

Authigenic titanium and zirconium minerals at the Verkhnekamskoe salt deposit. Geochemistry International, 57, 184–196.

Coleman, M.L. (1985) Geochemistry of diagenetic non-silicate minerals: kinetic considerations: Royal Society (of London), Philosophical Transactions, series A, 315, 39–56.

Ddani, M., Meunier, A., Zahraoui, M., Beaufort, D., El Wartiti, M., Fontaine, C., Boukili, B., El Mahi, B. (2005) Clay mineralogy and chemical composition of bentonites from the Gourougou volcanic massif (Northeast Morocco). Clays and Clay Minerals, 53, 250–267.

Dill, H.G. (2010) Authigenic heavy minerals a clue to unravel supergene and hypogene alteration of marine and continental sediments of Triassic to Cretaceous age (SE Germany). Sedimentary Geology, 228, 61–76.

Domingos, R.F., Tufenkji, N., Wilkinson, K.I. (2009) Aggregation of titanium dioxide nanoparticles: role of a fulvic acid. Environmental Science and Technology, 43(5), 1282–1286.

Ece, O.I., and Nakagawa, Z.E. (2003) Alteration of volcanic rocks and genesis of kaolin deposits in the Şile Region, northern İstanbul, Turkey. Part II: differential mobility of elements. Clay Minerals, 38, 529–550.

Fontaine, F., Christidis, G.E., Yans, J., Hollanders, S., Hoffman, A., Fagel, A. (2020) Characterization and origin of two Fe-rich bentonites from Westerwald (Germany). Applied Clay Science, 187, 105444.

Gallego-Urrea, J.A., Perez-Holmberg, J., Hassellöv, M. (2014) Influence of different types of natural organic matter on titania nanoparticles stability: effects of counter ion concentration and pH. Environmental Science: Nano, 1, 181–189.

Gao, Y., and Elder, S.A. (2000) TEM study of TiO_2 nanocrystals with different particle size and shape. Materials Letters, 44, 228–232.

Hochella, M.F. Jr., Mogk, D.W., Ranville, J., Allen, I.C., Luther, G.W., Marr, L.C., McGrail, B.P., Murayama, M., Qafoku, N.P., Rosso, K.M., Sahai, N., Schroeder, P.A., Vikesland, P., Westerhoff, P., Yang, Y. (2019) Natural, incidental, and engineered nanomaterials and their impacts on the Earth system. Science, 363, eaau8299.

Hochella, M.F. Jr., Lower, S.K., Maurice, P.A., Penn, R.L., Sahai, N., Sparks, D.L., Twining, B.S. (2008) Nanominerals, mineral nanoparticles, and Earth systems. Science, 319, 163–1635.

Hong, H.L., Algeo, T.J., Fang, Q., Zhao, L.L., Ji, K.P., Yin, K., Wang, C.W., Cheng, S. (2019)

Facies dependence of the mineralogy and geochemistry of altered volcanic ash beds: an example from Permian–Triassic transition strata in southwestern China. Earth-Science Reviews, 190, 58–88.

Hong, H.L., Jin, X.X., Wan, M., Ji, K.P., Liu, C., Algeo, T.J., Fang, Q. (2020) Occurrence of anatase in reworking altered ash beds (K-bentonites and tonsteins) and discrimination of source magmas: a case study of terrestrial Permian–Triassic boundary successions in China. Clay Minerals, 55, 329–341.

Hu, J., Li, C., Tong, J.N., Ye, Q., Tian, L., An, Z.H., Dodd, M.S., Algeo, T.J. (2020) Glacial origin of the Cryogenian Nantuo Formation in eastern Shennongjia area (South China): Implications for macroalgal survival. Precambrian Research, 351, 105969.

Inglès, M., and Ramos-Guerrero, E. (1995) Sedimentological control on the clay mineral distribution in the marine and non-marine Paleogene deposits of Mallorca (Western Mediterranean). Sediment. Geology, 94, 229–243.

Khalifa, M.A., and Morad, S. (2015) Impact of depositional facies on the distribution of diagenetic alterations in the Devonian shoreface sandstone reservoirs, Southern Ghadamis Basin, Libya. Sediment. Geology, 329, 62–80.

Liu, Z.R.R., Zhou, M.F., Williams-Jones, A.E., Wang, W., Gao, J.F. (2019) Diagenetic mobilization of Ti and formation of brookite/anatase in early Cambrian black shales, South China. Chemical Geology, 506, 79–96.

Lovley, D.R., Coates, J.D., Blunt-Harris, E.L., Phillips, E.J.P., Woodward, J.C. (1996) Humic substances as electron acceptors for microbial respiration. Nature, 382, 445–448.

Matthews, A. (1976) The crystallization of anatase and rutile from amorphous titanium dioxide under hydrothermal conditions. American Mineralogist, 61, 419–424.

Morad, S., and Aldahan, A.A. (1982) Authigenesis of titanium minerals in two proterozoic sedimentary rocks from southern and central Sweden. Journal of Sedimentary Petrology, 52, 1295–1305.

Pe-Piper, G., Karim, A., Piper, D.J.W. (2011) Authigenesis of titania minerals and the mobility of Ti: New evidence from pro-deltaic sandstones, Cretaceous Scotian basin, Canada. Journal of Sedimentary Research, 81, 762–773.

Pirlet, H., Wehrmann, L.M., Foubert, A., Brunner, B., Blamart, D., DeMol, L., VanRooij, D.,

Dewanckele, J., Cnudde, V., Swennen, R., Duyck, P. (2012) Unique authigenic mineral assemblages reveal different diagenetic histories in two neighbouring cold-water coral mounds on Pen Duick Escarpment, Gulf of Cadiz. Sedimentology, 59, 578–604.

Schroeder, P.A., and Shiflet, J. (2000) Ti-bearing phases in an east Georgia kaolin deposit. Clays and Clay Minerals, 48, 151–158.

Schulz, H., Wirth, R., Schreiber, A. (2016) Nano-crystal formation of TiO_2 polymorphs brookite and anatase due to organic-inorganic rock-fluid interactions. Journal of Sedimentary Research, 86, 59–72.

Símonarson, G., Sommer, S., Lotsari, A., Elgh, B., Iversen, B.B., Palmqvist, A.E.C. (2019) Evolution of the polymorph selectivity of titania formation under acidic and low-temperature conditions. ACS Omega, 4, 5750−5757.

Skrabal, S.A. (2006) Dissolved titanium distributions in the Mid-Atlantic Bight. Marine Chemistry, 102 (3-4), 218–229.

Strietzel, R., Hösch, R., Kalbfleisch, H., Buch, D. (1998) In vitro corrosion of titanium. Biomaterials, 19, 1495–1499.

Sugimoto, T., Zhou, X.P., Muramatsu, A. (2003) Synthesis of uniform anatase TiO_2 nanoparticles by gel–sol method 4. Shape control. Journal of Colloid and Interface Science, 259, 53–61.

Szczepanik, B. (2017) Photocatalytic degradation of organic contaminants over clay-TiO_2 nanocomposites: A review. Applied Clay Science, 141, 227–239.

Tilley, D.B., and Eggleton, R.A. (2005) Titanite low-temperature alteration and Ti mobility. Clays and Clay Minerals, 53, 100–107.

Weibel, R., and Friis, H. (2004) Opaque minerals as keys for distinguishing oxidizing and reducing diagenetic conditions in the Lower Triassic Bunter Sandstone, North German Basin. Sedimentary Geology, 169, 129–149.

Witham, C.S., Oppenheimer, C., Horwell, C.J. (2005) Volcanic ash-leachates: A review and recommendations for sampling methods. Journal of Volcanology and Geothermal Research, 141, 299–326.

Young, G.M., and Nesbitt, W.H. (1998) Processes controlling the distribution of Ti and Al in weathering profiles, siliciclastic sediments, and sedimentary rocks: Journal of Sedimentary Research, 68, 448–455.

Zhang, H., and Banfield, J.F. (1998) Thermodynamic analysis of phase stability of nanocrystalline titania. Journal of Materials Chemistry, 8, 2073–2076.

Zhang, H.Z., and Banfield, J.F. (2014) Structural characteristics and mechanical and thermodynamic properties of nanocrystalline TiO_2. Chemical Reviews, 114 (19), 9613–9644.

Acknowledgments

This work was supported by Natural Science Foundation of China (Projects 41972040 and 41472041). We thank Dr. Y.J. Li for the assistance in HRTEM observation, and J.S. Yu for the XRD analyses, and especially to Prof. W.D. Huff the Associate Editor, and the anonymous reviewers for their insightful reviews, valuable comments and suggestions. **Author contributions**: H.L.H. conceived, designed, and performed the research and wrote the paper. K.P.J., C.L., K.Y., L.L.Z., Q.F., and C.W.W. performed some aspects of the research. T.J.A and H.M. co-wrote and edited the paper. **Competing interests**: The authors declare no competing financial interests. **Data and materials availability**: All raw data and results including the images in Gatan DM ImageDocument format are available when request.